# Sensitivity of Electrical Inversion: A Numerical Experiment for $CO_2$ Monitoring

Amin Bassrei, CPGG/IGEO/UFBA & INCT-GP



## Abstract

Discussions on the effects of anthropogenic emissions of greenhouse gas and their consequences on climate change have gained public notoriety in recent decades. The capture of carbon dioxide ($CO_2$) from industrial sources and its subsequent storage in geological reservoirs can play an important role in reducing the harmful effects of the emission of this gas into the atmosphere. This study deals with the monitoring of geological reservoirs in the presence of $CO_2$ through the electrical resistivity method to estimate electrical properties of the rocks involved. Simulations performed on a four-layer synthetic model validated the applicability of the electrical method in monitoring $CO_2$ injection and leakage.

## Introduction

The global warming issue is one of the great challenges of humanity today, and the main problem is the fact that $CO_2$ absorbs thermal infrared light, thus being the main agent of the greenhouse effect. The harmful effects have encouraged the industry to reduction $CO_2$ emissions. One of the alternatives to mitigate the greenhouse effect, although costly, is the geological storage of carbon or CCS (Carbon Capture and Storage), which consists of storing $CO_2$ in appropriate sedimentary layers. The geological formations that can be used for CO2 storage are: (i) deep saline aquifers, (ii) depleted or non-depleted oil and gas reservoirs, and (iii) coal layers. Subsurface fluids fill the pore spaces of the rock, as do water, oil, natural gas and $CO_2$. The purpose of $CO_2$ geological storage is its injection into porous rock formations (Benson & Cole, 2008). Geological storage is based on the principle of returning $CO_2$ back underground. Therefore, $CO_2$ is stored in the lithosphere and its pore spaces. In these formations, CO2 can then be stored by different trapping mechanisms, depending on the relevant mechanism for the rock type. Oil reservoirs are proven geological traps, capable of retaining fluids and gases for a long period of time. The $CO_2$ injection technique for EOR – enhanced oil recovery has been a common practice in the oil industry for several decades and can be used in geological carbon storage. In reservoirs undergoing advanced recovery operations, the storage of a portion of the injected gas is a direct consequence of the use of $CO_2$ when the gas produced with the oil is captured and later injected into the reservoir. In this study, we use a non-seismic method called electrical resistivity prospection for monitoring $CO_2$ geological reservoirs. We consider a model of four parallel plane layers. The observed data are the apparent resistivity values, as a function of different offsets between the current electrodes. Those values are the input for the inversion procedure. The inversion output are the values of layer resistivity and thickness. To validate the methodology, the data were corrupted with random noise, so that the RMS deviation between the apparent resistivity and the apparent resistivity with noise was around 5%. The simulation results validated the 1-D approach of resistivity method, which showed sufficient sensitivity to evaluate the electrical properties of rocks involved in geological $CO_2$ storage.

## Electrical Properties and $CO_2$ Monitoring

The electrical resistivity of reservoir rocks is highly sensitive to variations in water saturation, according to Archie's equation (1942)

$$\rho_{rock} = \frac{\rho_{brine}}{\left(1 - S_{gas}\right)^2 \phi^2}, \qquad (1)$$

where $\rho_{rock}$ is the density of the rock as a function of gas saturation $S_{gas}$. On the other hand, $S_{gas} = 1 - S_{water}$, in which $S_{water}$ is the water saturation. $\rho_{brine}$ is the resistivity of the fluid in the pores (brine). All petroleum fluids (oil, condensate, and gas) and $CO_2$ are electrically resistive, so Archie's equation is appropriate (Gasperikova & Hoversten, 2006).

Archie's equation accurately describes the electrical resistivity of sedimentary rocks as a function of the listed parameters. It works well on clean and homogeneous sandstone. A key factor in resistivity measurements is the clay content, which produces a low apparent resistivity compared to actual resistivity because clay minerals tend to improve the path for electrical currents. The resistivity values increase during the gas injection period, but when calculated by the Archie equation, they present saturation around 10%. This number is less than that estimated from neutron log data. Such low saturation is assumed to be the effect of clay inclusion in the reservoir (Nakatsuka et al., 2010).

When $CO_2$ is injected into rock formations, the water in the porous space is displaced while reacting with this new element, forming carbonic acid. The coupling coefficient

evolves over time in response to mixing and pore water displacement.

As $CO_2$ displaces water, the coupling coefficient decreases. On average, the observed coupling coefficients for constant gas flow are about 10 times smaller than for water flow in the same sample. Since the coupling coefficient of liquid $CO_2$ is lower than that of water, the most effective way to monitor the spatial variation in the injected CO2 flow is to monitor the forward front of the $CO_2/H_2O$ ratio, where the coupling coefficient is greater (Hoversten & Gasperikova, 2005).

When the injected $CO_2$ reaches measurement zones, the resistivity increases considerably. The onset of increased resistivity indicates that $CO_2$ is migrating from the bottom to the upper end of the sandstone. There are differences in the $CO_2$ migration pattern due to the permeability and mineral composition of the rocks. In the case of clean and homogeneous sandstone, the fluid migrates as a uniform front in a relatively short period of time due to the high permeability. In contrast, heterogeneity and clay content decrease the displacement rate and make the process complex.

Gas saturation can be estimated from the initial resistivity of the rock fully saturated with brine (before the injection) and the resistivity of the partially saturated rock brine (during the injection) with the following equation:

$$S_{CO_2} = 1 - \left(\frac{1}{RI}\right)^{\frac{1}{n}}, \qquad (2)$$

where $RI$ is called resistivity index and $n$ is a numerical factor called saturation exponent. This relationship is empirical and was obtained through laboratory experiments carried out on sandstone samples from different reservoirs (Nakatsuka et al., 2010). $RI$ is defined as the ratio between the resistivity at a given instant of time and the initial resistivity, i.e. $RI = \rho / \rho_0$, hence that equation (2) can be written as

$$S_{CO_2} = 1 - \left(\frac{\rho_0}{\rho}\right)^{\frac{1}{n}}. \qquad (3)$$

Figure 1 shows the relationship between $CO_2$ saturation and the resistivity index $RI$, where the parameter $n$ = 1.62 was used, as suggested by Schmidt-Hattenberger et al. (2014).

The curve in Figure 1 is generic for any value of $\rho_0$. If we consider $\rho_0 = 100\ \Omega.\text{m},$ which corresponds to the resistivity of the rock 100% saturated with brine, we can present a curve of absolute resistivity values, as shown in Figure 2.

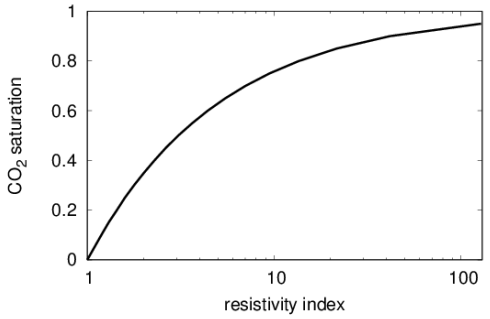


Figure 1: $CO_2$ saturation curve as a function of the resistivity index $RI$, with the index $n$ equal to 1.62.

On one hand, if $RI$ = 1.0, it follows that $\rho = \rho_0$ and the saturation is zero $(S_{CO_2} = 0),$ corresponding to the origin of the curve. On the other hand, a 95% saturation corresponds to $RI$ = 128.14, i.e. $\rho = 12{,}814\ \Omega.\text{m}.$ Moreover, Figure 2, which is specific for $\rho_0 = 100\ \Omega.\text{m},$ indicates the dynamics of the $CO_2$ injection process through arrows.

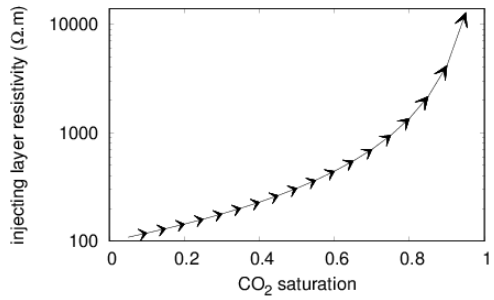


Figure 2: Absolute resistivity values as a function of $CO_2$ saturation, for $\rho_0 = 100\ \Omega.\text{m},$ which corresponds to the rock resistivity 100% saturated with brine. The dynamics of the $CO_2$ injection process is indicated by the arrows, with the final value $\rho = 12{,}814\ \Omega.\text{m},$ corresponding to a 95% $CO_2$ saturation.

**Simulations and Results**

Several simulations were performed on subsurface layered-models, using a 1-D approach. The results provide interpretations in a single dimension, in this case, along the depth axis.

To estimate the model parameters (layer resistivities and layer thicknesses), we employed the linearized inversion method described by Inman et al. (1973). In the present study, we applied the damped least squares method for the inversion, as proposed by Inman (1975). This method mitigates the ill-conditioned problem by damping the main diagonal of the matrix to be inverted, which is also sometimes called zeroth-order regularization. For the numerical procedure of the inversion, we used the decomposition by singular values.

There is an issue of ambiguity in the inversion process as it can provide solutions where the conductance (product between the thickness and the conductivity of a given layer) is constant while the individual thickness and/or conductivity values may vary.

The Schlumberger arrangement was chosen for this study due to its widespread use. We considered a four-layer model, with layers labeled A, B, C and D, from the uppermost to the lowest layer, with thicknesses are equal to 50 m. The layer resistivities are, from top to bottom, are 50, 100, 50, and 200 $\Omega.\mathrm{m}$.

Layer B, with $\rho_0 = 100\ \Omega.\mathrm{m}$, is initially saturated with 100% brine, characterizing the pre-injection condition. The solid curve of Figure 3 illustrates the apparent resistivity of this model. The gradual injection of $CO_2$ in layer B will imply a change in the apparent resistivity curve. Figure 3 depicts two additional curves representing the intermediate condition (with 50% $CO_2$ injection and 50% brine) and the post-injection condition (95% $CO_2$ injection and 5% brine).

The inversion was performed using the previously described algorithm. The observed data vector consisted of 15 values of apparent resistivity. The model parameters vector has 7 components: 4-layer resistivity values and 3-layer thickness values. Note that the fourth and last layer has a semi-infinite thickness. Therefore, the inverse problem is overdetermined, with $\mathrm{M}$ = 15 and $\mathrm{N}$ = 7. The vector of true model parameters is expressed as follows:

$$\mathbf{m}^{true} = (\rho_1, \rho_2, \rho_3, \rho_4, \Delta z_1, \Delta z_2, \Delta z_3). \qquad (4)$$

For methodology validation purposes, we introduced random noise to the apparent resistivity $\rho^a$ in the following formula:

$$\rho_i^{a,*} = \rho_i^a + \alpha r_i \rho_i^a, \qquad i = 1, \ldots, M, \qquad (5)$$

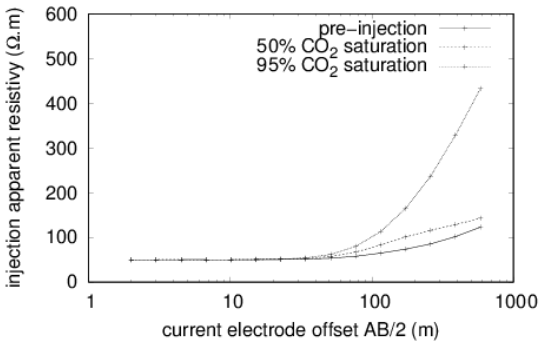


Figure 3: Apparent resistivity as a function of distance due to $CO_2$ injection in layer B, with $\rho_0 = 100\ \Omega.\mathrm{m}$. The solid curve describes the pre-injection condition, with 100% brine. The dashed curve represents the intermediate condition, with 50% $CO_2$ injection and 50% brine. The dotted curve depicts the post-injection condition, with 95% $CO_2$ injection and 5% brine.

in which $\rho^{a,*}$ is the apparent resistivity contaminated with noise; $\alpha$ is the noise factor and $r_i$ represents the random sequence. The value of $\alpha$ was chosen to ensure that the RMS deviation $\varepsilon_{rms}^{noise}$ between $\rho^{a,*}$ and $\rho^a$ is approximately 5%. This RMS estimator is expressed as follows:

$$\varepsilon_{rms}^{noise} = \frac{\sqrt{\sum_{i=1}^{M} (\rho_i^{a,*} - \rho_i^a)^2}}{\sqrt{\sum_{i=1}^{M} (\rho_i^a)^2}} \times 100\%. \qquad (6)$$

Figure 4 illustrates the apparent resistivity curves of $\rho^a$ and $\rho_i^{a,*}$. The electrode spacing was limited to 100 m to enhance the visibility of noise-induced fluctuations.

To perform the inversion, we required an a priori estimate of the model parameters. For this case, the priori model consisted of resistivity values equivalent to 80% of the true model and thickness values equal to the true values.

It is important to evaluate the proximity between the prior model and the true model in each simulation. For this purpose, we employed the RMS estimator of deviation between the true values of the model parameter $\mathbf{m}^{true}$ and the corresponding a priori values $\mathbf{m}^{prior}$ :

$$\varepsilon_{rms}^{prior} = \frac{\sqrt{\sum_{i=1}^{7} (m_i^{prior} - m_i^{true})^2}}{\sqrt{\sum_{i=1}^{7} (m_i^{true})^2}} \times 100\%. \qquad (7)$$

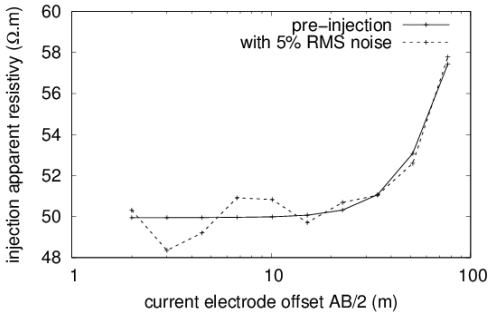


Figure 4: Curves of apparent resistivity $\rho^a$ and noise-contaminated apparent resistivity $\rho^{a,*}$. The RMS deviation between the two curves is $\varepsilon_{rms}^{noise}$ = 5%. The noise-caused fluctuation becomes more noticeable with the electrode spacing limited up to 100 m.

Similarly, for calculating the RMS deviation between the true model parameters $\mathbf{m}^{true}$ and the estimated model parameters $\mathbf{m}^{est}$, we used the following estimator:

$$\varepsilon_{rms}^{est} = \frac{\sqrt{\sum_{i=1}^{7}(m_i^{est} - m_i^{true})^2}}{\sqrt{\sum_{i=1}^{7}(m_i^{true})^2}} \times 100\%. \qquad (8)$$

Noisy resistivity values $\rho_i^{a,*}$ were used as input data for the inversion procedure. Figure 5 demonstrates the result in the $CO_2$ pre-injection condition, with layer B saturated with 100% brine. The RMS estimators are $\varepsilon_{rms}^{prior} = 3.52\%$ and $\varepsilon_{rms}^{est} = 0.90\%$.

Figure 6 displays the inversion result with noisy data for the intermediate condition, with 50% $CO_2$ injection and 50% brine. The RMS estimators are $\varepsilon_{rms}^{prior} = 3.80\%$ and $\varepsilon_{rms}^{est} = 0.19\%$.

Figure 7 exhibits the simulation for the final stage (post-injection condition), with 95% $CO_2$ injection and 5% brine in the same layer. In this final condition, the estimators provided $\varepsilon_{rms}^{prior} = 4.00\%$ and $\varepsilon_{rms}^{est} = 0.89\%$.

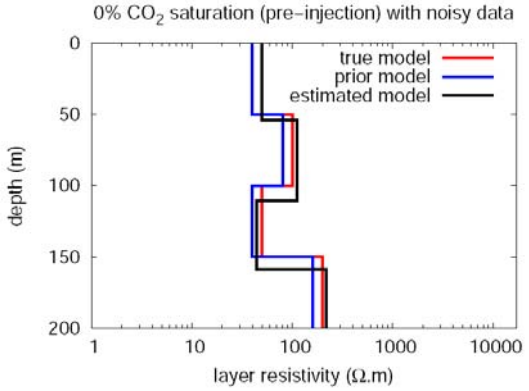


Figure 5: Inversion of apparent resistivity noisy data in the pre-injection condition, with layer B saturated with 100% brine.

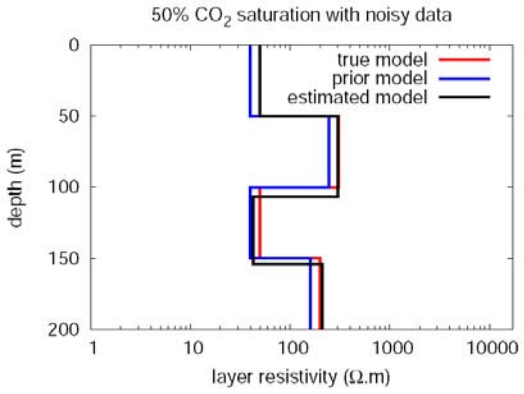


Figure 6: Inversion of apparent resistivity noisy data in the intermediate condition, with 50% $CO_2$ injection and 50% brine in layer B.

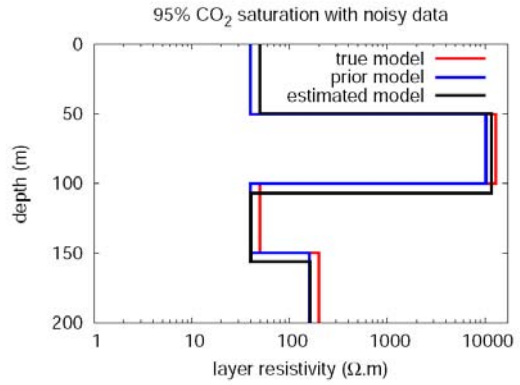


Figure 7: Inversion of apparent resistivity noisy data in the post-injection condition, with 95% $CO_2$ injection and 5% brine in layer B.

Despite the presence of noise, the results were quite satisfactory. As Figure 8 indicates, we integrated the different $CO_2$ injection stages.

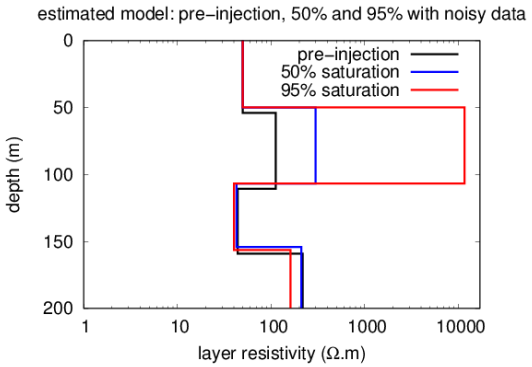


Figure 8: Estimated models at different stages of $CO_2$ injection.

The second set of simulations describes the $CO_2$ leaking condition, in which the brine replaces the $CO_2$. By using the same four-layer model, we now consider that the leakage occurs in layer C instead of layer B. We examined $CO_2$ saturations of 95%, 50% and 0%, with the complementary values summing up to 100% representing the brine saturation.

We consider the reference value of $\rho_0 = 6406.76\ \Omega.\mathrm{m}$ as the resistivity of layer C saturated with 95% $CO_2$. Figure 9 presents the absolute resistivity values, in which the arrows indicate the $CO_2$ leakage dynamics. In the final leakage step, with 0% CO2 saturation, we have $\rho = 50\ \Omega.\mathrm{m}$.

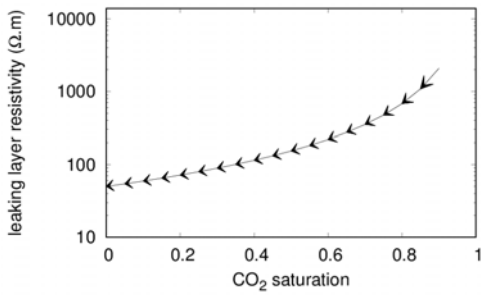


Figure 9: Absolute resistivity values as a function of $CO_2$ saturation, in which $\rho_0 = 6406.76\ \Omega.\mathrm{m}$ corresponds to the resistivity of rock saturated with 95% $CO_2$. The arrows indicate the dynamics of the $CO_2$ leakage process, with the final value $\rho = 50\Omega.\mathrm{m}$.

Figure 10 depicts the apparent resistivity curves. The solid curve represents the pre-leakage condition. The dashed curve illustrates the apparent resistivity in the intermediate condition, with 50% $CO_2$ injection and 50% brine. The dotted curve corresponds to the final condition of total $CO_2$ leakage, with 100% brine.

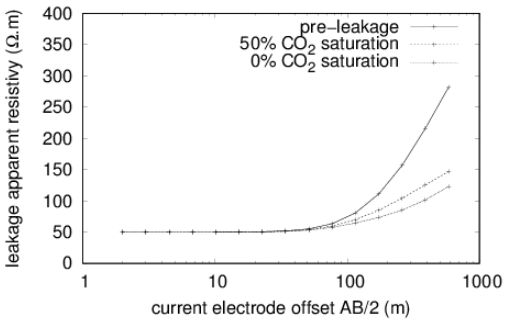


Figure 10: Change in apparent resistivity due to $CO_2$ leakage in layer C, with $\rho_0 = 6406.76\ \Omega.\mathrm{m}$. The solid curve depicts the pre-leakage condition, with the layer saturated with 95% $CO_2$. The dashed curve describes the intermediate condition, with 50% $CO_2$ injection and 50% brine. The dotted curve describes the post-leakage condition, with 100% brine.

Figure 11 illustrates the inversion of the apparent resistivity data in the pre-leakage condition, using the same a priori information. Despite the presence of noise, the estimated model remains very close to the true model. In quantitative terms, the RMS deviation between the true model and estimated model is $\varepsilon_{rms}^{est} = 0.81\%$.

Figure 12 presents the result of inverting the intermediate stage of leakage with the presence of noise. Interestingly, as observed in the $CO_2$ injection process, the RMS deviation between the true model and the estimated is $\varepsilon_{rms}^{est} = 0.14\%$ .

The result of inverting the final stage of leakage would be identical to the initial stage of the injection process (Figure 5). Finally, Figure 13 demonstrates the integration of the different stages of $CO_2$ leakage with the presence of noise.

## Conclusions

In this study, we verified the applicability of using 1-D electrical modeling and inversion for monitoring $CO_2$ storage. By measuring resistivity differences before, during and after gas injection, it is possible to monitor the gas dynamics in the subsurface. The simulation results in a four-layer model, including the presence of noise, aligned with our expectations, as evidenced by the overlapping curves of the injection or leakage in the different stages. With the presence of $CO_2$, the resistivity curve becomes more accentuated due to its higher resistance compared to other pore-filling fluids, such as water. The proposed methodology has been validated and proves its applicability to $CO_2$ geological storage, which offers a viable alternative to mitigate the environmental impacts of $CO_2$ emissions.

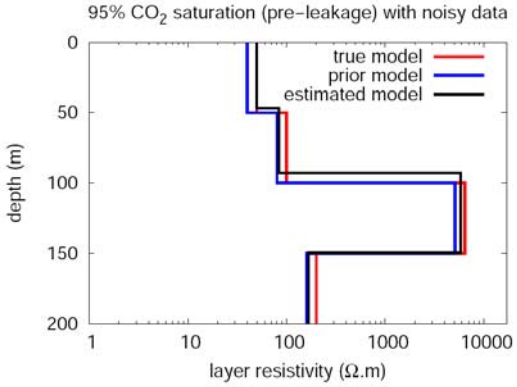


Figure 11: Inversion of apparent resistivity noisy data in the pre-leakage condition, with 95% $CO_2$ injection and 5% brine in layer C.

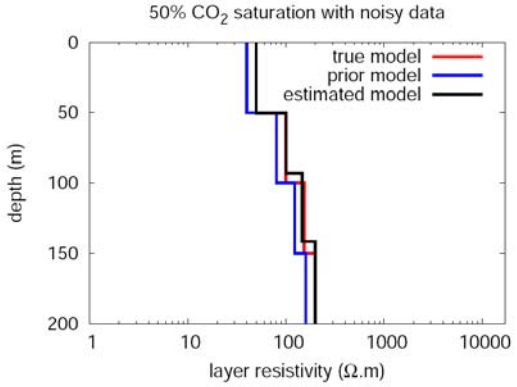


Figure 12: Inversion of apparent resistivity noisy data in the post-injection condition, with 50% $CO_2$ injection and 50% brine in layer C.

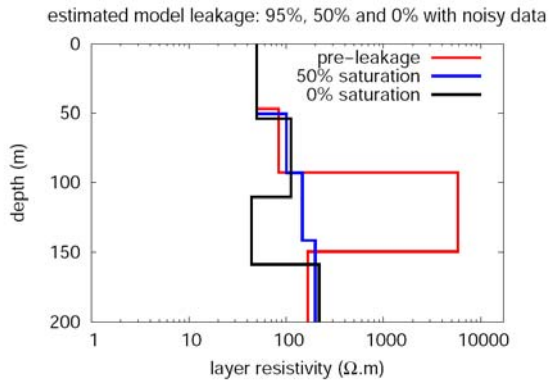


Figure 13: Estimated models of the different stages of $CO_2$ leakage with noise.

**Acknowledgments**

The author thanks the Conselho Nacional de Desenvolvimento Científico e Tecnológico (CNPq) for funding the Instituto Nacional de Ciência e Tecnologia de Geofísica do Petróleo (INCT-GP).

**References**

Archie, G., 1942, The electrical resistivity log as an aid in determining some reservoir characteristics: Transactions of the AIME, 146, 54-62.

Benson, S. M. & Cole, D. R., 2008, $CO_2$ sequestration in deep sedimentary formations, Elements, 4: 325-331.

Gasperikova, E. & Hoversten, G. M., 2006, A feasibility study of nonseismic geophysical methods for monitoring geologic $CO_2$ sequestration, The Leading Edge, 25: 1282–1288.

Hoversten, G. M. & Gasperikova, E., 2005, Non-seismic geophysical approaches to monitoring. In: Carbon Dioxide Capture for Storage in Deep Geologic Formations, vol. 2, Chapter 23, 1071-1112, D.C. Thomas and S.M. Benson (eds.), Elsevier: Amsterdam. ISBN: 9780080445700

Inman, J. R., 1975, Resistivity inversion with ridge regression, Geophysics, vol. 40, 798-817.

Inman, J. R., Ryu, J. & Ward, S. H. 1973, Resistivity inversion, Geophysics, vol. 38, 1088-1108.

Lazaratos, S. K. & Marion, B. P., 1997, Crosswell seismic imaging of reservoir changes caused by $CO_2$ injection, The Leading Edge, 16:1300-1308.

Nakatsuka, Y., Xue, Z., Garcia, H. & Matsuoka, T., 2010, Experimental study on $CO_2$ monitoring and quantification of stored $CO_2$ in saline formations using resistivity measurements, International Journal of Greenhouse Gas Control, 4:209-216.

Schmidt-Hattenberger, C., Bergmann, P., Labitzke, T. & Wagner, F., 2014, $CO_2$ migration monitoring by means of electrical resistivity tomography (ERT) - Review on five years of operation of a permanent ERT system at the Ketzin pilot site, Energy Procedia, 63: 4366-4373.